A Simple Method for Approximating the Optimal Trajectory

JAMES N. HANSON*
Battelle Memorial Institute, Columbus, Ohio

The equations of motion and the Euler equations for maximizing payload are combined. The resulting vector equation of this combination is linearized straightforwardly by selecting a constant value for the coefficients of derivatives of the dependent variable. The resulting equation is then a linear differential equation of the fourth order with constant coefficients. The solution, i.e., the radius vector $\mathbf{r}^*(t)$, is chosen to be dependent upon three parameters of the linearization, for whose values it is shown that, in the case of an Earth-Mars mission, $\mathbf{r}^*(t)$ is very insensitive. This trajectory then is compared to an absolute optimal solution of Irving and Blum and is seen to yield a terminal payload 30% less than theirs. A complete tabulation of this trajectory requires about 2 min on a Burroughs 205. This linearization exactly matches boundary conditions while appearing to be a feasible means of obtaining nonnegative payloads for a wide class of missions. In comparison, many steering programs when applied to the Irving and Blum mission yield negative payloads.

Nomenclature

a,b	= real and imaginary components of m_3 and m_4
a,b,c,d	= coefficients of the optimal equation of motions
α,β	= constants of integration for linearized solution
a.u.	= astronomical unit = 1.49504×10^8, km
γ	= space vehicle powerplant specific mass
ξ,η,ρ,λ	= parameters of linearization
θ	= transit angle
f	= vehicle acceleration produced by its powerplant
J	= $\frac{1}{2}\int_0^T f^2 dt$
k	= structural factor
M	= vehicle mass
μ	= sun's field strength = 39.47 8418 (a.u.^{3}-yr^{-2})
r	= heliocentric radius
t	= time
T	= transit time
U	= potential function
v	= heliocentric velocity
x^*	= pertains to the solution of linearization
$\mathbf{x}$	= vector
$\lvert\mathbf{x}\rvert$	= absolute value of
Δx	= incremental value of x
∇x	= gradient of x
$\mathbf{x}\cdot\mathbf{y}$	= vector dot production of $\mathbf{x}$ and $\mathbf{y}$
$<x>$	= the variable x has been replaced by the constant

Subscripts

0	= initial value
1	= terminal value
x	= x component
y	= y component

FOR power-limited flight, Irving and Blum have shown that, in order to maximize payload,[1] it is necessary to minimize J:

$$J = \frac{1}{2}\int_0^T f^2 dt \tag{1}$$

Received by IAS November 5, 1962; revision received May 7, 1963.

* Astronomer. Member AIAA.

where $\mathbf{f}$ is given by the equation of motion:

$$d^2\mathbf{r}/dt^2 = \mathbf{f} - \nabla U \tag{2}$$

For an inverse-square field,

$$U = \mu r^{-1} \qquad \nabla U = -\mu r^{-3}\mathbf{r} \tag{3}$$

Irving and Blum also have shown that, for an inverse-square field,[1] the Euler equations resulting from minimizing the integral of Eq. (1) are

$$\frac{d^2\mathbf{f}}{dt^2} + \frac{\mathbf{f}}{r^3} - \frac{3}{r^5}\mathbf{r}(\mathbf{f}\cdot\mathbf{r}) = 0 \tag{4}$$

If $\mathbf{f}$ is eliminated between Eqs. (2) and (4), then the following equation in $\mathbf{r}$ results:

$$\mathbf{r}^{IV} + r^{-3}\mathbf{r}^{III} - \mu r^{-3}\ddot{\mathbf{r}} + (6\mu r^{-4}\dot{r} - \mu r^{-6})\dot{\mathbf{r}} + (-12\mu r^{-5}\dot{r}^2 + 3\mu r^{-4}\ddot{r} + 3\mu r^{-3}\dot{r} - 3r^{-5}\mathbf{r}\cdot\dot{\mathbf{r}} + 3\mu r^{-6})\mathbf{r} = 0 \tag{5}$$

Let the respective coefficients of Eq. (5) be defined so that

$$\mathbf{r}^{IV} + a\mathbf{r}^{III} + b\ddot{\mathbf{r}} + c\dot{\mathbf{r}} + d\mathbf{r} = 0 \tag{6}$$

where a, b, c, and d are functions of $\mathbf{r}$, $\dot{\mathbf{r}}$, $\ddot{\mathbf{r}}$. Equation (6) is a linearization of Eq. (5). The solution of this linearization is the subject of this note. The solution of Eq. (6) for a given set of boundary conditions will be put into Newton's equation of motion, Eq. (2), to give the precise thrust program for the trajectory given by the linearized solution. If a, b, c, and d are evaluated for a given value of $\mathbf{r}$, $\dot{\mathbf{r}}$, $\ddot{\mathbf{r}}$ defined, respectively, by $\langle\mathbf{r}\rangle$, $\langle\dot{\mathbf{r}}\rangle$, $\langle\ddot{\mathbf{r}}\rangle$, then Eq. (6) becomes a linear fourth-order homogeneous equation with constant coefficients whose solution is of the form

$$\mathbf{r}^*(t) = \sum_{i=1}^{4} \boldsymbol{\alpha}_i e^{m_i t} \tag{7}$$

where $m_1, \ldots, m_4$ are the solutions of the characteristic equation

$$\prod_{i=1}^{4}(m - m_i) = m^4 + \langle a\rangle m^3 + \langle b\rangle m^2 + \langle c\rangle m + \langle d\rangle = 0 \tag{8}$$

By examination of typical values of $\langle\mathbf{r}\rangle$ for an Earth-Mars trajectory (namely the range of $\mathbf{r}$ covered between the initial and terminal radii), it has been found that the solution of Eq. (8) yields a complex pair. Therefore, Eq. (7) becomes

$$\mathbf{r} = \boldsymbol{\alpha}_1 e^{m_1 t} + \boldsymbol{\alpha}_2 e^{m_2 t} + e^{at}(\boldsymbol{\beta}_1 \cos bt + \boldsymbol{\beta}_2 \sin bt) \tag{9}$$

where the complex pair is defined by

$$m_3 = a + bi \qquad m_4 = a - bi \tag{10}$$

Let T be the mission time; then the initial and terminal conditions for an orbital transfer may be written as

$$\begin{aligned} \mathbf{r}(0) &= \mathbf{r}_0 = \mathbf{r}_0^* & \dot{\mathbf{r}}(0) &= \mathbf{v}_0 = \mathbf{v}_0^* \\ \mathbf{r}(T) &= \mathbf{r}_1 = \mathbf{r}_1^* & \dot{\mathbf{r}}(T) &= \mathbf{v}_1 = \mathbf{v}_1^* \end{aligned} \tag{11}$$

The conditions of Eqs. (11), when applied to Eq. (9), yield the following set of linear equations in the variables $\boldsymbol{\alpha}_1$, $\boldsymbol{\alpha}_2$, $\boldsymbol{\beta}_1$, $\boldsymbol{\beta}_2$:

$$\begin{bmatrix} \boldsymbol{\alpha}_1 \\ \boldsymbol{\alpha}_2 \\ \boldsymbol{\beta}_1 \\ \boldsymbol{\beta}_2 \end{bmatrix} = \begin{bmatrix} 1 & 1 & 1 & 0 \\ m_1 & m_2 & a & b \\ e^{m_1 T} & e^{m_2 T} & e^{aT}\cos bT & e^{aT}\sin bT \\ m_1 e^{m_1 T} & m_2 e^{m_2 T} & ae^{aT}\cos bT - be^{aT}\sin bT & ae^{aT}\sin bT + be^{aT}\cos bT \end{bmatrix}^{-1} \times \begin{bmatrix} \mathbf{r}_0 \\ \mathbf{v}_0 \\ \mathbf{r}_1 \\ \mathbf{v}_1 \end{bmatrix} \tag{12}$$

Therefore, Eqs. (8, 9, and 12) define a trajectory that exactly matches the boundary conditions of Eqs. (11). This trajectory has as parameters the choice for the values of $\langle \mathbf{r} \rangle$, $\langle \dot{\mathbf{r}} \rangle$, and $\langle \ddot{\mathbf{r}} \rangle$, which permits the linearization of Eq. (5) by assigning constant values to a, b, c, and d.

The actual function $\mathbf{r}(t)$, which gives the absolute minimum for J, is the solution of Eq. (5). Hence, the usefulness of Eq. (9) will be determined by how closely it approximates the solution of Eq. (5) or by how closely the J computed by the solution of Eq. (5) is approximated by J^*. The latter case of comparing J with J^* will be examined.

Let the values of $\langle \mathbf{r} \rangle$, $\langle \dot{\mathbf{r}} \rangle$, and $\langle \ddot{\mathbf{r}} \rangle$ be denoted as follows:

$$\xi = \langle r \rangle \qquad \eta = \langle \dot{r} \rangle \qquad \rho = \langle \ddot{r} \rangle \qquad \lambda = \langle r^{-1}\mathbf{r}\cdot\ddot{} \rangle \tag{13}$$

Then the constant values of a, b, c, and d, corresponding to a set of ξ, η, ρ,λ, are given by

$$\begin{aligned} \langle a \rangle &= \xi^{-3} \\ \langle b \rangle &= -\mu\xi^{-3} \\ \langle c \rangle &= 6\mu\xi^{-4}\eta - \mu\xi^{-6} \\ \langle d \rangle &= -12\mu\rho^{-5}\eta^2 + 3\mu\xi^{-4}\rho + 3\mu\rho^{-7}\eta - 3\xi^{-4}\lambda + 3\mu\xi^{-6} \end{aligned} \tag{14}$$

Irving and Blum numerically integrated Euler's equations and the equations of motion [i.e., they numerically solved Eq. (5)], using the following initial conditions[2]:

$$\begin{aligned} r_{0x} &= 1 && && \text{(a.u.)} \\ r_{0y} &= 0 && && \text{(a.u.)} \\ v_{0x} &= 6.283 && 1853 && \text{(a.u.-yr}^{-1}\text{)} \\ v_{0y} &= 0 && && \text{(a.u.-yr}^{-1}\text{)} \end{aligned} \tag{15}$$

Their terminal values for the trial integration coming closest to matching the Martian perhelion were

$$\begin{aligned} r_{1x} &= 1.329 && 6400 && && \text{(a.u.)} \\ r_{1y} &= 0.391 && 3340 && 0 && \text{(a.u.)} \\ v_{1x} &= 1.572 && 0800 && && \text{(a.u.-yr}^{-1}\text{)} \\ v_{1y} &= -5.341 && 4700 && && \text{(a.u.-yr}^{-1}\text{)} \end{aligned} \tag{16}$$

where this corresponds to a transit angle and transit time given by

$$\theta = 73°.6 \qquad T = 0.25 \text{ (yr)} \tag{17}$$

The initial choices for the parameters of Eq. (13) may be obtained from their mean values

$$\begin{aligned} \xi &= \langle r \rangle = \tfrac{1}{2}[|\mathbf{r}_0| + |\mathbf{r}_1|] \\ \eta &= \langle \dot{r} \rangle = \tfrac{1}{2}[|\mathbf{v}_0| + |\mathbf{v}_1|] \\ \rho &= \langle \ddot{r} \rangle = \eta T^{-1} \\ \lambda &= \langle r^{-1}\mathbf{r}\cdot\ddot{\mathbf{r}} \rangle = \tfrac{1}{2}[r_0^{-1}\mathbf{r}_0\cdot\mathbf{v}_0 + r_1^{-1}\mathbf{r}_1\cdot\mathbf{v}_1]T^{-1} \end{aligned} \tag{18}$$

For the Irving and Blum Martian mission given by Eqs. (15–17), ξ, η, and λ are

$$\begin{aligned} \xi &= 1.193 && 0186 && \text{(a.u.)} \\ \eta &= 3.141 && 5926 && \text{(a.u.-yr}^{-1}\text{)} \\ \lambda &= 0.591 && 5564 && \text{(a.u.-yr}^{-2}\text{)} \end{aligned} \tag{19}$$

The absolute minimum J obtained by Irving and Blum and by the values in Eq. (19) are, respectively,

$$\begin{aligned} J &= 0.0317 && \text{(kw-kg}^{-1}\text{)} \\ J^* &= 0.0430 && \text{(kw-kg}^{-1}\text{)} \end{aligned} \tag{20}$$

The values of $J^* = J^*(\xi,\eta,\rho,\lambda)$ were computed for the ranges $1.0 \leq \xi \leq 1.7$, $0 \leq \eta \leq 0.3$, $0 \leq \rho \leq 20$, and $0 \leq \lambda \leq 20$; J^* was found to be very *insensitive* to the choices of ξ, η, ρ, λ for these wide ranges about the mean values given in Eq. (19). The minimum J^* is 0.0426, which differs slightly from that given in Eq. (20) by the parameters of Eq. (19). This minimum was found by varying ξ, η, ρ, and λ over a wide range of values. Hence, by a relatively simple calculation (requiring 2 min on a Burroughs 205), an Earth-Mars transfer orbit is obtained which yields a terminal J, 1.35 times the absolute minimum terminal J (whose computation required extensive numerical integration of the equations of motion and Euler's equations).

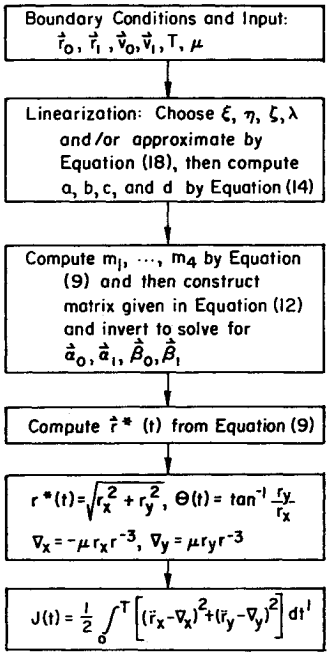

Fig. 1 Flow chart for computing $\mathbf{r}^*(t)$, $\mathbf{f}^*(t)$, $J^*(t)$.

The payload fraction and J are related by[1]

$$M_L/M_0 = \{[1 - (\gamma J)^{1/2}]^2 - k\}/(1 - k) \tag{21}$$

where the mass of the power supply is not included in the payload. If the structural factor k is assumed to be negligible, then, for a given specific weight γ, the relative variation in M_L/M_0 resulting from a variation in J is approximated by

$$\frac{\Delta(M_L/M_0)}{(M_L/M_0)} \approx \frac{-(\gamma J)^{1/2}}{1 - (\gamma J)^{1/2}}\left(\frac{\Delta J}{J}\right) \tag{22}$$

Hence, if $\Delta J/J = 0.35$ and $J = 0.04$ (kw-kg^{-1}), then, for $\gamma = 5$ (kg-kw^{-1}), the relative variation in payload is 30% (i.e., the linearization performed herein yields a payload 30% less than the absolute maximum).

At first sight, it would appear that an approximation differing by 30% from the true solution would be of little value. However, when the trajectory $\mathbf{r}^* = \mathbf{r}^*(t)$ obtained by this linearization is compared with other steering programs, it is found that J^* is an order of magnitude smaller. For example, if the steering programs described by Rodriquez[3] are applied to the boundary conditions in Eqs. (15–17), a negative payload will result for a realistic structural factor, say $k = 0.05$.

In conclusion, it may be conjectured that the linearization described herein provides an approximate solution (which exactly matches boundary conditions). For missions "similar" to or less ambitious than the Earth-Mars transfer, it yields a trajectory resulting in a payload that is probably within 30% of the absolute maximum attainable, whereas for the general mission it might be expected that $\mathbf{r}^*(t)$ would yield nonnegative payloads without undertaking the lengthy numerical solution of Eq. (5) or its equivalent.

Figure 1 contains a flow chart for computing $\mathbf{r}^*(t)$, $\mathbf{f}^*(t)$, $J^*(t)$.

References

[1] Irving, J. H., "Low-thrust flight: variable exhaust velocities in gravitational fields," *Space Technology*, edited by H. Seifert (John Wiley and Sons Inc., New York, 1959), Chap. 10.

[2] Irving, J. H. and Blum, E. K., "Comparative performance of ballistic and low-thrust vehicles for flight to Mars," *Second*

Annual AFOSR Astronautic Symposium, Denver, Colo. (April 1958).

[3] Rodriquez, E., "Method for determining steering programs for low thrust interplanetary vehicles," ARS J. 29, 783–788 (1959).

Shock-Wave Boundary-Layer Interaction on a Missile Nose Probe

M. D. Bennett*
Sandia Corporation, Albuquerque, N. Mex.

When a pressure probe is mounted on the nose of a missile, a compression corner is formed at the juncture of the probe base and vehicle nose. At supersonic speeds, the shock wave emanating from the compression corner interacts with the probe boundary layer to produce perturbations both downstream and upstream from the corner. To avoid flow interference at the pressure orifice, the afterbody of the probe must be sufficiently long that the orifice is located upstream of the shock-wave boundary-layer interaction region. Wind-tunnel tests were made to determine the critical length for a cone-cylinder probe at speeds from Mach 1.4 to 4.0 and freestream unit Reynolds numbers from 7.0×10^5 to 8.0×10^6/ft. In transitional flow with adiabatic wall temperature, the afterbody critical length is proportional to Mach number and angle of attack and inversely proportional to Reynolds number. In turbulent flow, the critical length is relatively small and apparently independent of Mach number, Reynolds number, and angle of attack.

Introduction

In some flight applications, a small probe is mounted on the nose of a missile to permit measurement of atmospheric properties such as pressure or density. At supersonic speeds, a shock wave emanates from the region where the probe joins the nose section of the vehicle. The abrupt increase in pressure through the shock wave results in a strong, adverse pressure gradient that can cause separation of the probe boundary layer. Consequently, the pressure distribution both downstream and upstream from the compression corner may be affected. If the extent of the shock-wave boundary-layer interaction in the upstream direction is sufficient to cause interference with flow at the probe orifice, measured pressure (or density) will be affected. In the extreme cases, the interference effect can amount to more than 50% of the true pressure. To eliminate flow interference, the afterbody of the probe may be made sufficiently long that the orifice is upstream of the interaction region.

Numerous studies of separated flow at supersonic speeds have been reported. The results indicate that any of the many variables that affect transition location can influence the extent of, and pressure distribution in, separated flow regions. Thus, in addition to the variables previously mentioned, surface roughness, stream turbulence, heat transfer, probe geometry, and vehicle nose geometry can affect the critical length of the probe afterbody.

Most of the previous studies have been concerned with the separated region in two-dimensional flows. The present study is concerned with the length of the separated flow ahead of a compression corner in an axially symmetric flow. Data at angles of attack up to 12° are presented.

Received January 29, 1963.

* Supervisor, Aerophysics Section.

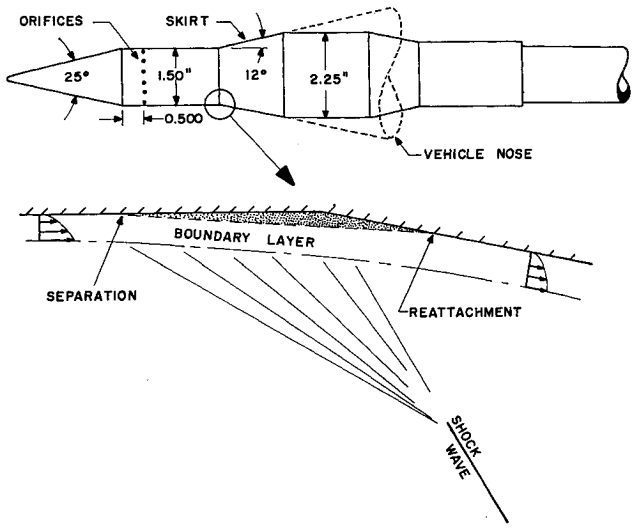

Fig. 1 Sketch of wind-tunnel model for shock-wave boundary-layer interaction tests.

Experiment

Tests were performed in a 12- × 12-in. wind tunnel at speeds from Mach 1.4 to Mach 4.0; freestream Reynolds number (V_0/ν_0) range was approximately 7.0×10^5 to 8.0×10^6/ft. The geometry of the pressure probe and an exaggerated sketch of the shock-wave boundary-layer interaction are shown in Fig. 1. The model was supported by a swept strut attached to the side wall of the tunnel. The leading edge of the strut was located about 2.5 in. downstream of the broken section shown at the right-hand margin in Fig. 1. The probe was fixed with respect to the tunnel, and the axial position of the skirt (the forward section of which represents the tip of the vehicle nose) was remotely controlled. The diameter of the skirt was made sufficiently large that the reattachment point was located on the forward section of the skirt; the reattachment point was determined from schlieren photographs and spark shadowgraphs. Clearance between the skirt lip and the cylindrical section of the probe was about 0.004 in. There were 24 $\frac{1}{16}$-in.-diam orifices located $\frac{1}{2}$ in. downstream from the cone-cylinder shoulder and equally spaced around the periphery of the probe. The orifices were manifolded in a tube located on the axis of the

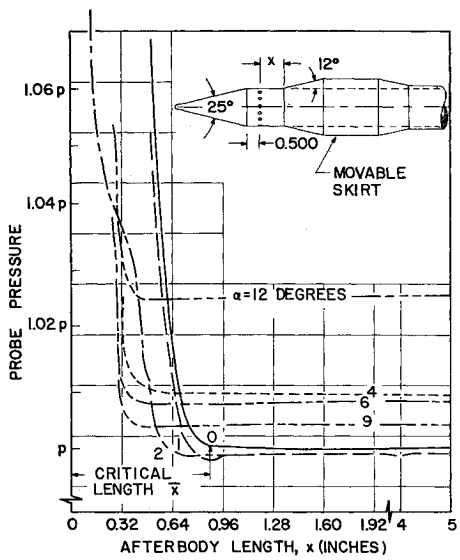

Fig. 2 Effect of skirt position on probe pressure at Mach 1.4 ($V_0/\nu_0 = 0.58 \times 10^6$/in.).